ADVANCED MATERIALS
www.advmat.de

www.MaterialsViews.com

Progress of Flexible Electronics in Neural Interfacing – A Self-Adaptive Non-Invasive Neural Ribbon Electrode for Small Nerves Recording

*Zhuolin Xiang, Shih-Cheng Yen, Swathi Sheshadri, Jiahui Wang, Sanghoon Lee, Yu-Hang Liu, Lun-De Liao, Nitish V. Thakor, and Chengkuo Lee**

Neuroprostheses enable the communication between the nervous system and artificial devices so that a diseased neurological function can be restored, replaced, or modulated. A key component for the clinical applicability of neuroprostheses is the neural interface; the device intends to extract information from the nervous system that can be used to control a prosthetic apparatus, map brain functions, and treat neural disorders.[1–3] Microdevices fabricated by microelectromechanical systems (MEMS) technology have replaced fine metal wires as advanced neural interfaces thanks to their high spatial resolution, dimensional accuracy, and promising scalability. In terms of device configuration, these neural interfaces can be classified into two main groups, namely, invasive microneedle-like electrodes and non-invasive sheet electrodes. For example, the Michigan probe[4] and Utah array[5] electrodes are the most well-known microneedle-like electrodes, whereas the cuff electrode[6] and flexible multiplexed electrode array[7] are representatives for sheet electrodes. As a reactive glial sheath will encapsulate the neural interface and further hinder neural stimulation and recording after the invasive implantation process, non-invasive sheet electrodes are more preferable for practical in vivo testing.[8]

Among these non-invasive sheet electrodes in **Table 1**,[9–16] conventional electrode devices made of rigid structures and materials cannot provide long-term and robust interfaces with neurons, neural fascicles, and nerves. The mechanical mismatch between these stiff substrates and soft tissue[17] aggravates micromotion at the tissue–electrode contact sites, which will induce inflammation inside the tissue.[18] To solve this problem, polymer materials, such as SU-8,[19] parylene,[20] polyimide,[21] liquid crystal polymer,[22] silk,[23] and benzocyclobutene (BCB),[24] are employed to fabricate flexible neural interfaces. As these materials can change shape when the neural tissue deforms, flexible neural interfaces made of these materials can avoid a gradual shift in recording location and a decrease in the signal to noise ratio. For flexible peripheral nerve interfaces, J. A. Hoffer and G. E. Loeb reported their pioneering work in the 1970s with successful neural signal recording by cuff electrodes and platinum wires on a walking cat.[25,26] After that, P. E. K Donaldson et al. improved the flexibility of cuff electrodes with silicone rubber[27] and optimized the electrical parameters for better communication with the peripheral nerve system.[28] By implementing subspace separation algorithms, T. Sinkjaer et al. demonstrated improved signal recording with cuff electrodes in a very noise environment.[29,30] N. Donaldson et al. reported tripolar recording on a cuff electrode, which reduced the electromyography (EMG) signal interference and enhanced the recorded electroneurogram (ENG) signals in the experiment.[31–33] They also achieved velocity-selective recording by determining the velocity spectrum information from recorded ENG signals with a cuff electrode. J. Struijk and L. Andreasen showed that an optimized configuration and closure of the cuff electrode contributes to the neural signal acquisition.[34,35] T. Stieglitz et al. developed processing technology for flexible, light-weight, micromachined, multichannel cuff electrodes.[36] With this device, X. Navarro et al. were able to selectively stimulate the fascicular of a rat's sciatic nerve.[37] The cuff electrode has also been reported to control the blood pressure by selective stimulation of the vagal nerve.[38]

However, even the most commonly used polymer peripheral nerve interface, the cuff electrode, still has two main challenges to overcome: 1) dimension-adaptiveness to record signals from nerves with different diameters and 2) capability to communicate with very fine nerves at the distal end (e.g., the diameter is less than 300 μm).

The main drawback for current cuff electrodes is that they are based on a split cylinder with a fixed diameter, which cannot properly fit nerves of different sizes. As the diameters of peripheral nerves in the body are randomly distributed and may vary over a range of a hundred micrometers, predefined

Z. Xiang, Prof. S. C. Yen, S. Sheshadri, J. Wang, S. Lee, Y. H. Liu, Prof. N. V. Thakor, Prof. C. Lee
Department of Electrical & Computer Engineering
National University of Singapore
4 Engineering Drive 3, 117576, Singapore
E-mail: elelc@nus.edu.sg

Z. Xiang, Prof. S. C. Yen, S. Sheshadri, J. Wang, S. Lee, Y. H. Liu, Dr. L.-D. Liao, Prof. N. V. Thakor, Prof. C. Lee
Singapore Institute for Neurotechnology (SiNAPSE)
National University of Singapore
28 Medical Drive, #05-COR, 117456, Singapore

Z. Xiang, J. Wang, S. Lee, Prof. C. Lee
Center for Intelligent Sensors and MEMS
National University of Singapore
4 Engineering Drive 3, 117576, Singapore

Prof. N. V. Thakor
Department of Biomedical Engineering
School of Medicine
Johns Hopkins University Baltimore
MD 21205, USA

DOI: 10.1002/adma.201503423

Table 1. Comparison of representative neural interfaces.

		Microneedle-like (Invasive)	Sheet-like (Non-invasive)
For central nervous system	Rigid	Silicon neural probe integrated with sensors[9]	Glass plane microelectrode array[10]
	Flexible	Ultra thin flexible neural probe[11]	Graphene based electrode array[12]
For peripheral nervous system	Rigid	Slanted Utah array[13]	Metal wire monopolar electrode[14]
	Flexible	Transverse intrafascicular multichannel electrode[15]	Cuff electrode[16]

cuff electrodes usually do not match perfectly with these nerves. A cuff electrode that is too small may induce a serious compression on the nerve, which will cause injury during chronic implantation,[39] whereas a cuff electrode that is too large can only be loosely attached to the nerve whereby the main concern is the poor contact between the electrical sites and the target nerve.[40] Moreover, to record neural signals with a high spatial specificity, the existing cuff electrodes reach their limit in handling the targeting of fine nerves with diameters less than 300 µm.[41] Even though cuff electrodes are technically flexible devices, the stiffness of the platinum wires that are embedded inside the polydimethylsiloxane (PDMS) sleeves still prevent the cuff electrode from fully conforming to the small nerve. When the electrode is required to provide a tailored and stable contact with a small nerve, the assembly of thin metal wires in a small, curved PDMS tube is expected to be inaccurate and suboptimal.

Here, we demonstrate a flexible and biocompatible neural ribbon electrode that can achieve self-adaption to nerves with various diameters, communicates with small nerves, and shows 3D contacting for non-invasive implantations. This new electrode was innovatively wrapped around the nerve with fixed sutures at two ends. Its unique spiral wrapping mechanism allowed the device to match with nerves of different diameters, which avoids the poor communication between the contacts and the nerve bundles that generally occurs in conventional cuff electrodes. As the whole thickness of the polyimide device was only 10 µm, integrating 200 nm of electrical tracing, it fully conforms to small nerve bodies and we were able to show neural recording from rat sciatic nerve branches of very small diameters. The 3D protruding electrodes coated with carbon nanotubes (CNTs) further enabled a close contact that was non-invasive, to provide good communication between the electrical sites and the underlying nerves.

The design of the polyimide-based neural ribbon electrode is illustrated in **Figure 1**a. It is a strip-like device and mainly consists of five sections. Firstly, there are two front-end suturing holes at one terminal of the ribbon, which are used to fix the front part on the surface of the epineurium. After that eight 3D circular protruding electrical contacts, 150 µm in diameter, are placed on a 1.4 cm long stripe. This part serves as the main body of the device to communicate with the nerve bundles. Then a 200 µm × 500 µm reference electrode and four rear-end suturing holes lie on two small wings. The four suturing holes here are designed to fix the rear part of the device on the epineurium. In order to minimize the interference from the connector during implantation, a 0.5 cm long transition part is intentionally added between the connection pad and the

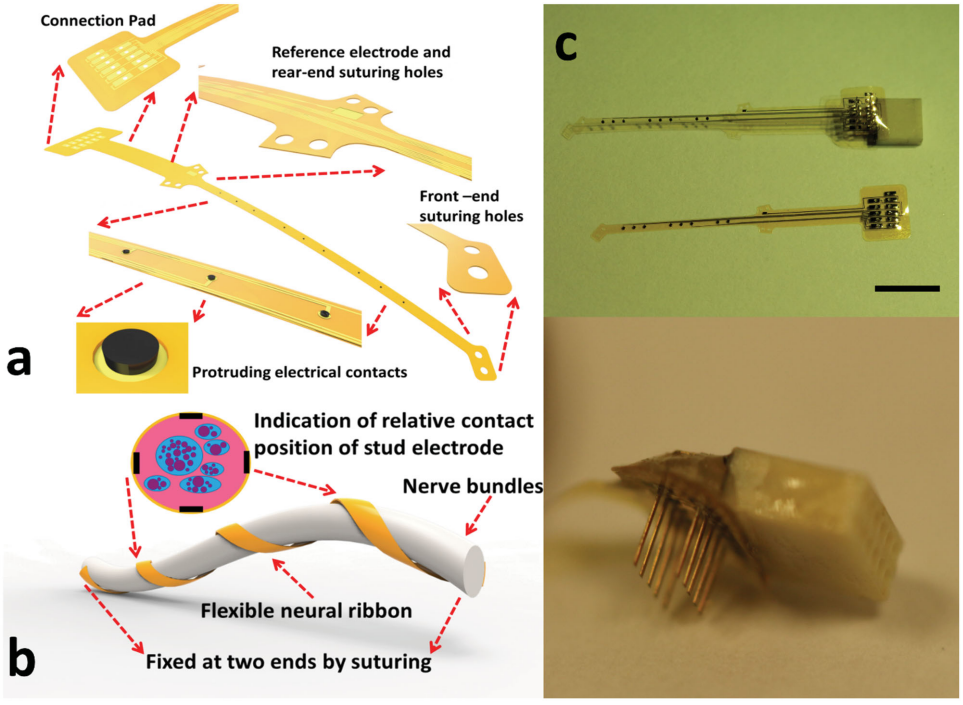

Figure 1. a,b) Illustration of the design of a neural ribbon electrode and its implantation. c) Optical image of the fabricated device (scale bar: 5mm).

rear-end suturing holes. At the other terminal of the ribbon, a special connection pad with holes is designed to match a customized connector. In the implantation procedure, the neural ribbon device is designed to be attached on the nerve as shown in Figure 1b. The front-end suturing holes are used to fix the front part of the neural ribbon on the nerve. With this part fixed, the neural ribbon can then be wrapped helically along the nerve because of the high flexibility of the ultra-thin polyimide substrate.[11] The type of polyimide used was Durimide and has been proven to be stable under long-term strain-stress testing.[42] The wrapping process does not induce unfavorable cracks into the substrate. Moreover, the 3D circular protruding electrical contacts of the neural ribbon electrode directly touch the epineurium surface, which establishes an excellent communication between the sensing contacts and the activated nerve bundles. The detailed fabrication process and assembly method are provided in the Supporting Information.

After the devices were released from the substrate and attached with an Omnetics connector (Figure 1c), a layer of CNTs was coated on the 3D SU-8 protruding contacts to increase the effective surface area and improve the charge transfer at the electrode–tissue interface. Electrophoretic deposition (EPD) was employed to deposit the CNT film as it is an automated and high-throughput process that generally produces films with a good homogeneity and packing density.[43] When an electrical voltage is applied, the Au ions in the solution, as well as the CNTs, as they absorb Au ions, migrated to the negative terminals. After collecting electrons from the protruding contacts, the Au ions subsequently deposit on the contact surface (**Figure 2**a). The CNTs with a diameter of 0.5–2 μm and a length of less than 8 μm also adhered to the Au electrode contacts by the same process (Figure 2b). The difference between a Au electrode contact and a CNT-coated contact is shown in Figure 2c,d. Impedance spectroscopy of both the Au contacts and CNT-coated contacts showed that at the biologically relevant frequency of 1 kHz, the impedance of the Au electrode and the CNT-coated electrode were 285.47 kΩ and 6.2 kΩ, respectively. This demonstrates that the resistance of the 3D electrodes of the fabricated neural ribbon are significantly improved by the electroplating with CNTs. Apart from the low electrical impedance, the neural ribbon electrode also showed a reversible linear elongation when the applied strain was less than 7%. Owing to the ultrathin polyimide layers, the bending stiffness of the fabricated device was less than 200 N μm^{-2}, which was conducive to the wrapping process in the in vivo experiments (testing and calculations are provided in the Supporting Information).

In order to prove that the neural ribbon can be matched with nerves of different diameters and be applied to small nerves, three terminal branches of sciatic nerves of different diameters (300–600 μm), peroneal nerves, tibial nerves, and sural nerves were chosen to be implanted with the fabricated devices. The successful results are shown in **Figure 3**a. To assess the nerve-recording capabilities of the neural ribbon, acute recording experiments were conducted using the fabricated devices on a sciatic nerve of Sprague-Dawley rats (250–400 g). The experimental set-up for evoking and recording the compound action potentials (CAPs) on the nerve is demonstrated in Figure 3b. CAPs were evoked by delivering 20 μs cathodic monophasic pulses of varying current (0.2–0.7 mA) through two hooked platinum electrodes using a Digitimer. The responses evoked under the varying stimulus parameters were recorded by the distal neural ribbon electrodes. To prove the recording capability of the fabricated neural ribbon electrodes on small nerves with different diameters, four neural ribbon devices were implanted on the surface of a sciatic nerve, a peroneal nerve, a tibial nerve, and a sural nerve, respectively. Differential recordings of the CAPs were taken from contacts on each neural ribbon electrode with respect to an Ag/AgCl wire sutured under the skin beside the surgical site. 60 evoked CAPs per second were recorded and averaged to reduce the noise. Complex waveforms were observed in these stimulated CAPs. Figure 3c showed a representative signal recorded from one of the channels on the electrode. According to the study presented by Mathews et al.,[44] the recorded signal was divided into four parts. The stimulation was delivered at time 0 and the corresponding stimulus artifact appeared immediately. The stimulus artifact varied in duration and amplitude based on the stimulus intensity and pulse width applied through the hook stimulation

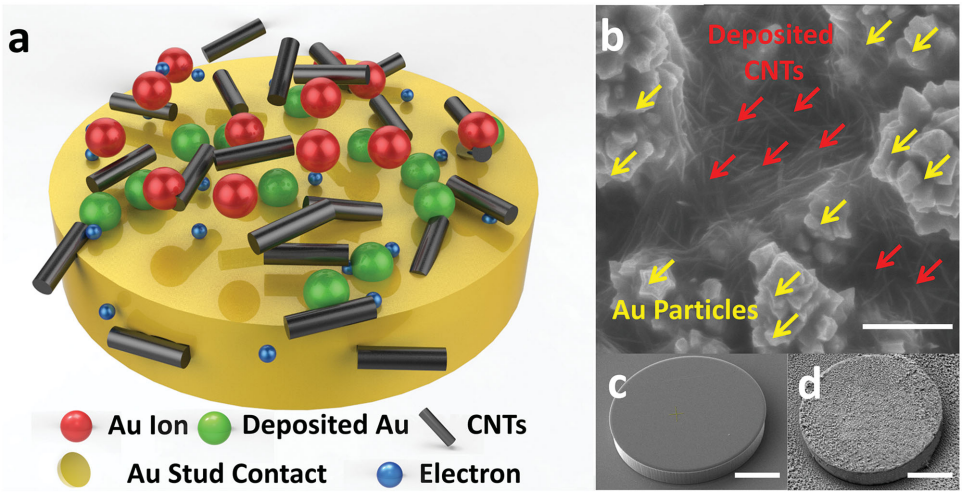

Figure 2. a) Schematic drawing for the CNTs electroplating process. b) Details of the deposition of CNT and Au particles. c) SEM image for CNT-coated 3D electrode.

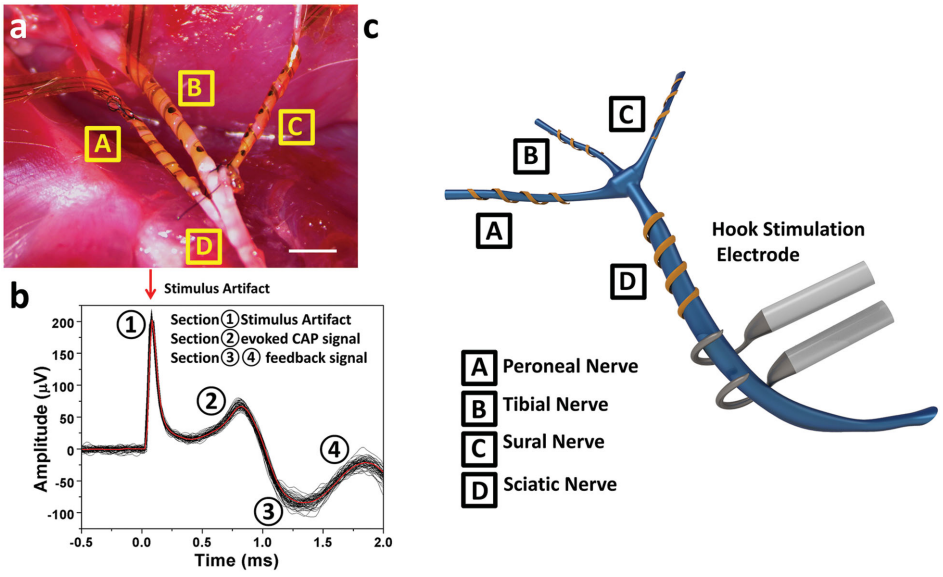

Figure 3. a) Implantation of a neural ribbon and acute recording in vivo (scale bar = 1 mm). b) Representative evoked neural signal. c) Illustration of the in vivo testing setup.

electrode. The following peak was defined as the directly evoked CAP signal conducted by the nerve, which is marked as section 2 in the figure. Section 3 and section 4 in Figure 3c represent information feedback from the muscles or sensory neurons after conduction of the stimulation.

The recorded signals under 0.6 mA stimulation from 4 different neural ribbon electrodes are shown in **Figure 4**. Figure 4a shows the signal that was recorded from the sciatic nerve. All 8 contacts on the neural ribbon were apparently activated but the amplitudes were different. As the faciculus has

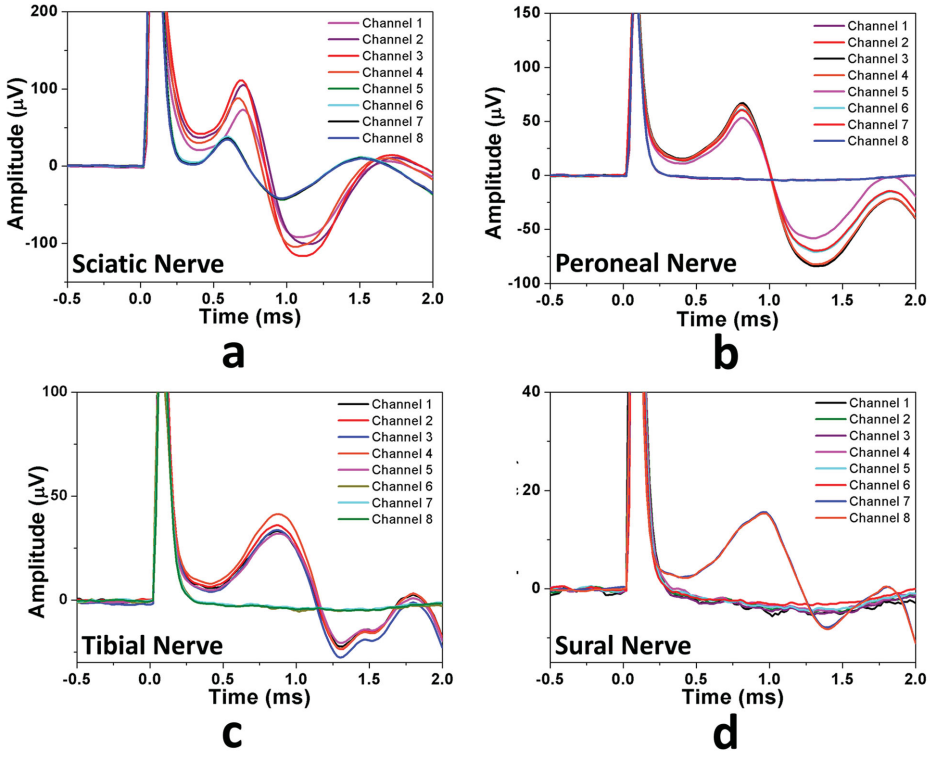

Figure 4. The recorded signals under 0.6 mA stimulation from: a) sciatic nerve, b) peroneal nerve, c) tibial nerve, and d) sural nerve. The data is averaged from 60 recordings.

ADVANCED MATERIALS
www.advmat.de

Materials Views
www.MaterialsViews.com

an anisotropic distribution under the epineurium, the distance between the sensing contacts on the neural ribbon and the active fascicles varied at different locations. Thus, even under the same stimulation, the conductive current density received by the contacts was different. Moreover, not all the contacts of the neural ribbon electrodes, which were implanted on the three branch terminals, could be activated. Figure 4b,c shows that only some of the channels could record neural activities. Especially on the smallest nerve, the sural nerve, only two channels were activated. As the nerve faciculus in the sciatic nerve splits into three portions, the number of fascicles inside the branch terminals is smaller than that in the sciatic nerve. Therefore, when the nerves are stimulated under the same current, the number of activated fascicles was the lowest in the small sural nerve. Only the contacts that were close enough to the faciculus in the sural nerve receive sufficient current to record any signals. That is why only two channels can record signals in the neural ribbon electrode that was attached on the sural nerve. This result also indicates that multiple contacts on the electrode increases the chance to record neural signals.

The peak value of the neural activity was recorded under increasing stimulus intensity (from 0.2 mA to 0.7 mA). The results are shown in **Figure 5**. Figure 5a shows the recording amplitude from the sciatic nerve whereas Figure 5b–d present the recorded amplitudes from the peroneal nerve, tibial nerve, and sural nerve, respectively. The evoked CAPs were the algebraic summation of all the action potentials produced by all the fascicles within the nerve bundles excited by the electrical stimulation. When the stimulation current was lower than 0.3 mA, only a few fascicles were activated and most of the contacts on the neural ribbon electrodes did not record any signal. When the stimulus current increased, more fascicles were activated. Thus more action potentials were added up to produce a higher amplitude signal as all the contacts on the neural ribbon electrode recorded larger signals. However, when the stimulus current increased to a certain point (around 0.55 mA in this case), all fascicles were activated, and the corresponding recorded amplitudes reached a threshold. No matter how much more the stimulus current was increased, the recorded amplitudes remained constant.

During the acute test, the latency value and the distance between the stimulating sites and recording electrodes were also measured to calculate the nerve conduction velocity. The latency for the measured CAP signal in each implanted neural ribbon was obtained under the stimulations with different currents. As the neural activity measured in region 2 of Figure 3b was the most consistent for neural recording, therefore this region was used for tracking the latency on different neural ribbons over the experimental period. The results are shown in **Figure 6**. The neural ribbon implanted on the sciatic nerve was the closest to the stimulation hook electrodes. The signal latency recorded by the neural ribbon on the sciatic nerve was smaller than that recorded by neural ribbons attached to the branch terminals. However, when stimulated by different currents, the latencies in all of the neural ribbon electrodes almost remained constant. The conduction velocity of single fibers only depended on its diameter and the nerve bundles were composed of fibers of varying diameters. Fast fibers with larger

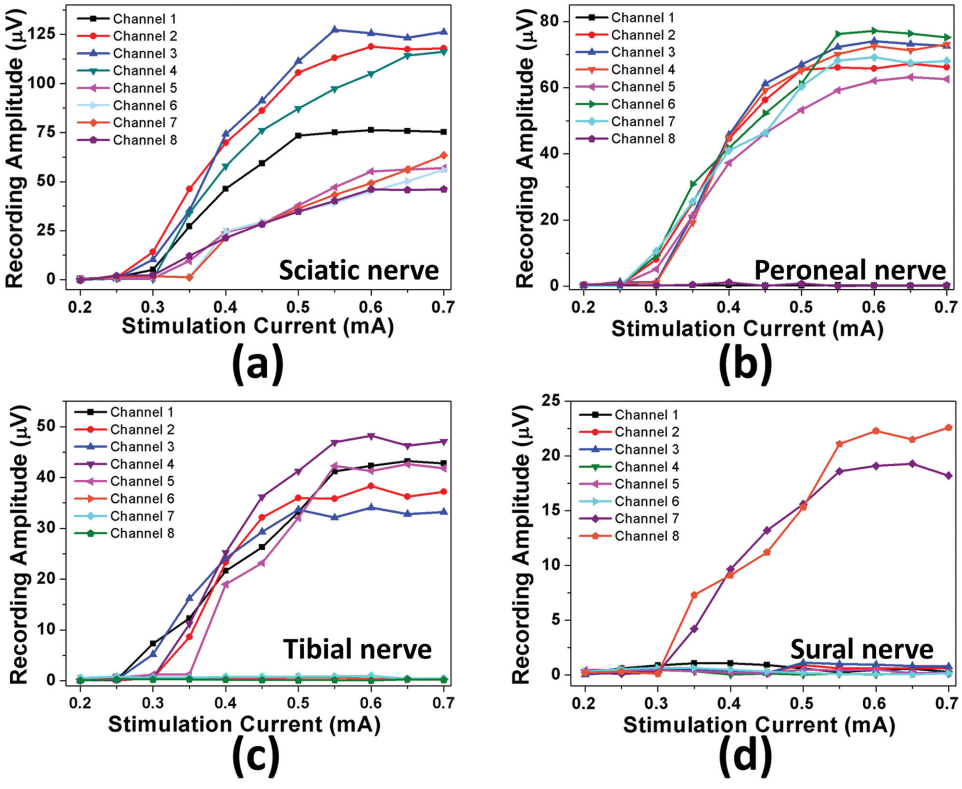

Figure 5. The peak value of neural activity was recorded with increasing stimulus intensity in: a) sciatic nerve, b) peroneal nerve, c) tibial nerve, and d) sural nerve.

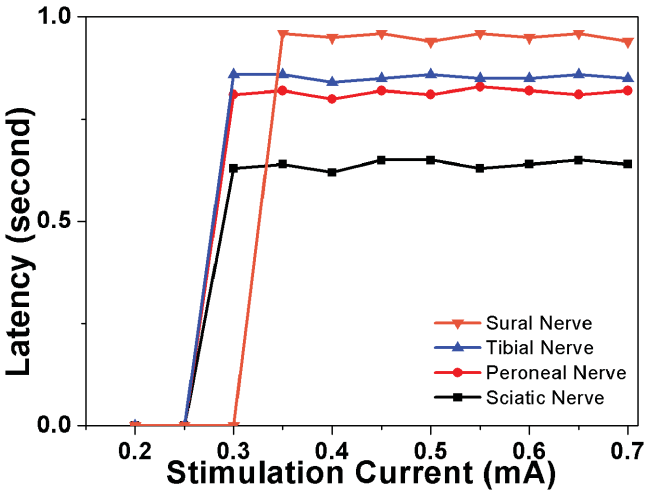

Figure 6. Neural signals latency on different neural ribbons over the experimental period.

diameters possessed action potentials that fell in the region towards the start of the CAP whereas slower fibers with smaller diameters had action potentials that fell in the tail section region. As long as the fibers in the nerve bundle were activated, the conduction velocity was fixed but the signal wave shape and duration may increase with rising stimulus. The conduction velocity of the neural ribbon electrode that was implanted on the sciatic nerve, which was 3 cm away from the stimulation site, was around 46 m s^{-1}, which is in agreement with the values reported by Stanley et al.[45]

As the neural ribbon electrode is wrapped on the nerve surface, the main concern for a wide acceptance of this device is potential injury due to the compressive pressure. Before the induced pressure is large enough to physically damage the nerve tissues, the blood flow in the connective vessels decreases predominantly due to the compression.[46] To investigate the influence of the implanted neural ribbon before and after the device attachment, we applied functional photoacoustic microscopy (fPAM) to evaluate the formation and hemodynamic changes of the nerve before and after electrode implantation. Photoacoustic (PA) imaging is an emerging bio-photonic imaging technique that overcomes the resolution drawbacks of pure optical imaging and possesses the merits of both optics and ultrasound – namely, high optical absorption contrast and sub-millimeter ultrasound resolution – up to an imaging depth of centimeters.[47] Our experimental data of the formation and hemodynamic changes of the nerve are shown in **Figure 7**a–c before (upper layer) and after (lower layer) electrode implantation. The hand-microscope images in Figure 7a indicate that no significant formation change is seen in the nerve after electrode implantation, which was confirmed by the ultrasound images in Figure 7b. More importantly, as shown in Figure 7c, our PA data indicated that under the same region of interest (ROI), there were no significant PA signal changes after electrode implantation. Overall, based on our ultrasound and PA data, no significant changes were reported in either the formation and hemodynamics of the nerve before and after electrode implantation.

In summary, a neural ribbon electrode was successfully implanted on nerves of various diameters (300–600 μm) in rats by wrapping around these nerves with suturing at two ends. It is the first time that neural signals were passed between nerves from the rat's sciatic nerve branches, such as the peroneal nerve, tibial nerve, and sural nerve, and these signals were successfully recorded in a non-invasive way, which cannot be achieved by conventional extraneural electrodes. With these unique capabilities, neural ribbon electrodes are promising to specifically control target organs by only communicating with those closely connected to fine nerves. This will be helpful to establish a highly sensitive, instant, and precise feedback to understand unknown electroceutical mechanisms.

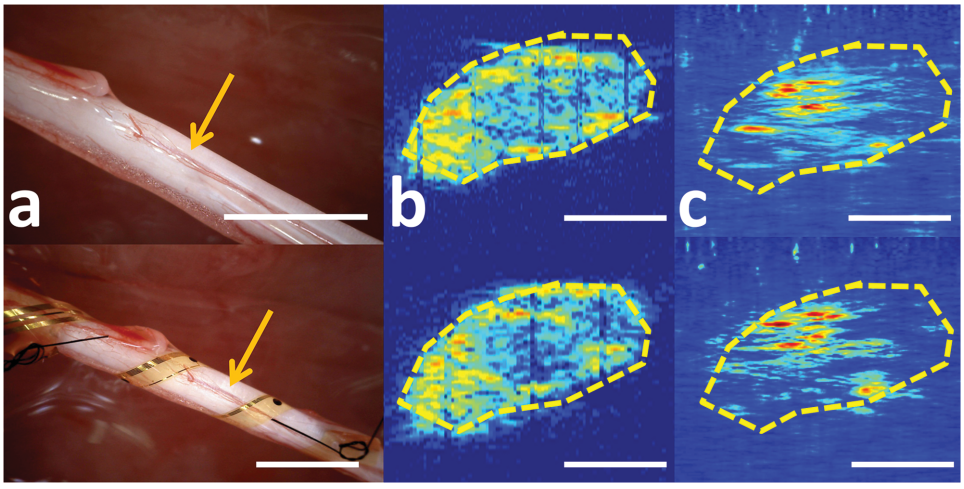

Figure 7. a,b) Evaluation of influence to the sciatic nerve induced by neural ribbon implantation. c) Optical image before and after neural ribbon electrode implantation. The orange arrows indicate the location for photoacoustic microscopy, scale bar = 1 mm. d) Ultrasound images to compare the blood vessel status on the nerve before (top) and after the implantation (bottom). e) Photoacoustic image to compare the blood vessel status on the nerve before (top) and after the implantation (bottom).

Experimental Section

CNTs Electroplating: The multiwall CNTs (Cheap Tubes Inc. US) were first dispersed in a Au electrolyte bath TSG-250 (Transene, US) to form a 1 mg mL^{-1} aqueous solution. Then the whole solution was sonicated for 2 h to suspend the CNTs fully in the solution. After that, the packaged neural ribbon device and a Au wire were connected to the negative terminal and the positive terminal of the power supply, respectively. Both the probe tip and the Au wire were then dipped into the solution. A monophasic voltage pulse with 1 V amplitude and 50% duty cycle was applied to the power source. The Au ions in the solution as well as the CNTs, which absorbed Au ions, migrated to the negative terminal. After reduction with the electrons from the protruding contacts, a Au/CNTs layer was deposited on the contact surface.

Implantation of the Neural Ribbon: Sprague-Dawley rats (250–400 g) were used for the sciatic nerve implantations. Anesthesia was induced using a mixture of Xylazine (7.5 mg/kg IP) and Ketamine (50 mg/kg IP) in 0.9% NaCl. After the animals were fully anesthetized, the legs were shaved from the knee to the hip using an electrical shaver. The surgery field was disinfected with chlorhexidine and 70% ethanol. Then the femur of the rat was found using one's forefinger and an incision of approximately 0.5 cm parallel and approximately 1.5 mm anterior to the femur was made using a surgical blade. The underlying fat was removed and the muscles close to the femur were separated with two autoclaved sticks. When the embedded sciatic nerve was visible, the attached fat was removed using a surgical forceps. A 9–0 suture with a curved needle was put through one of the front-end suturing holes. The curved needle penetrated the epineurium and took the suture into the nerve tissue. Then the curved needle was returned from the other front-end suturing hole and a knot was tied to fix this front part on the nerve bundles. With this part fixed, the neural ribbon device was then wrapped along the nerve helically. After making sure that all the recording contacts touched the nerve surface, the rear-end suturing holes were used to fix the other end of the neural ribbon. All the procedures were performed under protocol 143/12 and approved by the Institutional Animal Care and Use Committee in the National University of Singapore.

Photoacoustic Image Measurement: The sciatic nerves of the rats were imaged using a 50-MHz dark-field confocal PAM system with 32×61 μm^2 resolution. An optical parametric oscillator pumped by a frequency-tripled Nd:YAG Q-switched laser was employed to provide laser pulses of around 4 ns at a pulse repetition rate of 10 Hz. The laser energy was delivered using a 1-mm multimode fiber. The fiber tip was coaxially aligned with a convex lens, an axicon, a plexiglass mirror, and an ultrasonic transducer on an optical bench, forming dark-field illumination that was confocal with the focal point of the ultrasonic transducer. Laser pulses at 570 nm were used for the PA wave excitation of the total hemoglobin (HbT) content. A large numerical-aperture, wideband 50-MHz ultrasonic transducer was employed to allow the efficient collection of the PA signals. The scanning step size was 20 μm for each B-scan. The PA signals received by the ultrasonic transducer were pre-amplified by a low-noise amplifier (noise Figure 1.2 dB, gain 55 dB, AU-3A-0110, Miteq, USA), cascaded to an ultrasonic receiver (5073 PR, Olympus, USA), then digitized and sampled by a computer-based 14-bit analog to digital (A/D) card (CompuScope 14200, GaGe, USA) at a 200-MHz sampling rate for data storage. Fluctuations in the laser energy were monitored by a photodiode (DET36A/M, Thorlabs, USA). Recorded photodiode signals were applied to compensate for the PA signal variations caused by the instability in the laser energy before any further signal processing.

Supporting Information

Supporting Information is available from the Wiley Online Library or from the author.

Acknowledgements

This work was supported by grants from the National Research Foundation (NRF) CRP project 'Self-Powered Body Sensor Network for Disease Management and Prevention Oriented Healthcare (NRF2011 NRF-CRP001–057)' (R-263–000-A27–281) and the National Research Foundation (NRF) CRP project 'Peripheral Nerve Prostheses: A Paradigm Shift in Restoring Dexterous Limb Function (NRF-CRP10–2012–01)' (R-719–000–001–281).

Received: July 16, 2015
Revised: September 17, 2015
Published online: November 16, 2015

[1] K. Famm, B. Litt, K. J. Tracey, E. S. Boyden, M. Slaoui, *Nature* **2013**, *496*, 159.
[2] S. J. Bensmaia, L. E. Miller, *Nat. Rev. Neurosci.* **2014**, *15*, 313.
[3] W. M. Grill, S. E. Norman, R. V. Bellamkonda, *Annu. Rev. Biomed. Eng.* **2009**, *11*, 1.
[4] K. D. Wise, D. J. Anderson, J. F. Hetke, D. R. Kipke, K. Najafi, *Proc. IEEE* **2004**, *92*, 76.
[5] E. M. Maynard, C. T. Nordhausen, R. A. Normann, *Electroencephalogr. Clin. Neurophysiol.* **1997**, *102*, 228.
[6] G. G. Naples, J. T. Mortimer, A. Scheiner, J. D. Sweeney, *IEEE Trans. Biomed. Eng.* **1988**, *35*, 905.
[7] J. Viventi, D.-H. Kim, L. Vigeland, E. S. Frechette, J. A. Blanco, Y.-S. Kim, A. E. Avrin, V. R. Tiruvadi, S.-W. Hwang, A. C. Vanleer, *Nat. Neurosci.* **2011**, *14*, 1599.
[8] A. B. Schwartz, X. T. Cui, D. J. Weber, D. W. Moran, *Neuron* **2006**, *52*, 205.
[9] E. G. R. Kim, H. Tu, H. Luo, B. Liu, S. Bao, J. Zhang, Y. Xu, *Lab Chip* **2015**, *15*, 2939.
[10] A. B. Kibler, B. G. Jamieson, D. M. Durand, *J. Neurosci. Methods* **2012**, *204*, 296.
[11] Z. Xiang, S.-C. Yen, N. Xue, T. Sun, W. M. Tsang, S. Zhang, L.-D. Liao, N. V. Thakor, C. Lee, *J. Micromech. Microeng.* **2014**, *24*, 065015.
[12] D.-W. Park, A. A. Schendel, S. Mikael, S. K. Brodnick, T. J. Richner, J. P. Ness, M. R. Hayat, F. Atry, S. T. Frye, R. Pashaie, *Nat. Commun.* **2014**, *5*.
[13] H. C. Wark, R. Sharma, K. S. Mathews, E. Fernandez, J. Yoo, B. Christensen, P. Tresco, L. Rieth, F. Solzbacher, R. Normann, P. Tathireddy, *J. Neural Eng.* **2013**, *10*, 045003.
[14] D. J. Tyler, D. M. Durand, *IEEE Trans. Neural Syst. Rehabil. Eng.* **2002**, *10*, 294.
[15] T. Boretius, J. Badia, A. Pascual-Font, M. Schuettler, X. Navarro, K. Yoshida, T. Stieglitz, *Biosens. Bioelectron.* **2010**, *26*, 62.
[16] C. Veraart, W. M. Grill, J. T. Mortimer, *IEEE Trans. Biomed. Eng.* **1993**, *40*, 640.
[17] J. N. Turner, W. Shain, D. H. Szarowski, M. Andersen, S. Martins, M. Isaacson, H. Craighead, *Exp. Neurol.* **1999**, *156*, 33.
[18] R. Biran, D. C. Martin, P. A. Tresco, *J. Biomed. Mater. Res. A* **2007**, *82*, 169.
[19] S.-H. Cho, H. M. Lu, L. Cauller, M. Romero-Ortega, J.-B. Lee, G. Hughes, *Sensors J. IEEE* **2008**, *8*, 1830.
[20] S. Takeuchi, D. Ziegler, Y. Yoshida, K. Mabuchi, T. Suzuki, *Lab Chip* **2005**, *5*, 519.
[21] S. Takeuchi, T. Suzuki, K. Mabuchi, H. Fujita, *J. Micromech. Microeng.* **2004**, *14*, 104.
[22] S. E. Lee, S. B. Jun, H. J. Lee, J. Kim, S. W. Lee, C. Im, H. Shin, J. W. Chang, S. J. Kim, *IEEE Trans. Biomed. Eng.* **2012**, *59*, 2085.
[23] D.-H. Kim, J. Viventi, J. J. Amsden, J. Xiao, L. Vigeland, Y.-S. Kim, J. A. Blanco, B. Panilaitis, E. S. Frechette, D. Contreras, *Nat. Mater.* **2010**, *9*, 511.
[24] K. Lee, J. He, R. Clement, S. Massia, B. Kim, *Biosens. Bioelectron.* **2004**, *20*, 404.
[25] G. E. Loeb, M. J. Bak, J. Duysens, *Science* **1977**, *197*, 1192.

[26] J. A. Hoffer, G. E. Loeb, *Ann. Biomed. Eng.* **1980**, *8*, 351.
[27] P. E. K. Donaldson, *Med. Biol. Eng. Comput.* **1991**, *29*, 34.
[28] N. Donaldson, P. E. K. Donaldson, *Med. Biol. Eng. Comput.* **1986**, *24*, 41.
[29] B. Upshaw, T. Sinkjær, *Rehabil. Eng. IEEE Trans.* **1998**, *6*, 172.
[30] J. O. Larsen, M. Thomsen, M. Haugland, T. Sinkjær, *Acta Neuropathol.* **1998**, *96*, 365.
[31] M. Rahal, J. Winter, J. Taylor, N. Donaldson, *IEEE Trans. Biomed. Eng.* **2000**, *47*, 1281.
[32] I. F. Triantis, A. Demosthenous, N. Donaldson, *Biomed. Eng. IEEE Trans.* **2005**, *52*, 314.
[33] A. Demosthenous, J. Taylor, I. F. Triantis, R. Rieger, N. Donaldson, *Circuits Syst. I Regul. Pap. IEEE Trans.* **2004**, *51*, 629.
[34] L. N. S. Andreasen, J. J. Struijk, *Biomed. Eng. IEEE Trans.* **2002**, *49*, 1045.
[35] L. N. S. Andreasen, J. J. Struijk, in *Engineering in Medicine and Biology Society, Proc. IEEE* **1998**, Vol. *6*, pp. 3004–3007.
[36] T. Stieglitz, M. Schuettler, J.-U. Meyer, *Biomed. Microdevices* **2000**, *2*, 283.
[37] X. Navarro, E. Valderrama, T. Stieglitz, M. Schüttler, *Restor. Neurol. Neurosci.* **2001**, *18*, 9.
[38] D. T. T. Plachta, M. Gierthmuehlen, O. Cota, N. Espinosa, F. Boeser, T. C. Herrera, T. Stieglitz, J. Zentner, *J. Neural Eng.* **2014**, *11*, 036011.
[39] D. K. Leventhal, D. M. Durand, *IEEE Trans. Biomed. Eng.* **2004**, *51*, 1649.
[40] D. R. McNeal, B. R. Bowman, *Med. Biol. Eng. Comput.* **1985**, *23*, 249.
[41] J. S. Ordonez, V. Pikov, H. Wiggins, C. Patten, T. Stieglitz, J. Rickert, M. Schuettler, in *36th Annual Int. Conf. IEEE: Eng. Med. Biol. Soc.* **2014**, pp. 6846–6849.
[42] B. Rubehn, T. Stieglitz, *Biomaterials* **2010**, *31*, 3449.
[43] B. Gao, G. Z. Yue, Q. Qiu, Y. Cheng, H. Shimoda, L. Fleming, O. Zhou, *Adv. Mater.* **2001**, *13*, 1770.
[44] K. S. Mathews, H. C. Wark, R. Normann, *Muscle Nerve* **2014**, *50*, 417.
[45] E. F. Stanley, *Exp. Neurol.* **1981**, *71*, 497.
[46] M.-S. Ju, C.-C. K. Lin, J.-L. Fan, R.-J. Chen, *J. Biomech.* **2006**, *39*, 97.
[47] L. V. Wang, *IEEE J. Sel. Top. Quantum Electron.* **2008**, *14*, 171.